Bridging Bis-Bidentate Coordination of the Usually Tetradentate 5,7,12,14-Tetramethyldibenzo[*b*,*i*][1,4,8,11]tetraazacyclotetradecine Macrocyclic Ligand: Experimental and Theoretical Study of $[Mo_2(O_2CR)_2(C_{22}H_{22}N_4)]$. Comparative Electrochemical Behavior of the [Mo$\overset{4}{-}$Mo] Core

J. M. Kerbaol,[1a] E. Furet,[1b] J. E. Guerchais,*[,1a] Y. Le Mest,[1a] J. Y. Saillard,*[,1b] J. Sala-Pala,[1a] and L. Toupet[1c]

Unité Associée au CNRS 322, Laboratoire de Chimie, Electrochimie Moléculaires et Chimie Analytique, Université de Bretagne Occidentale, 29287 Brest Cedex, France, Unité Associée au CNRS 254, Laboratoire de Chimie du Solide et Inorganique Moléculaire, Université de Rennes I, 35042 Rennes Cedex, France, and Unité Associée au CNRS 804, Groupe Matière Condensée et Matériaux, Université de Rennes I, 35042 Rennes Cedex, France

Received March 18, 1992

Treatment of the dimolybdenum tetracarboxylato derivatives $[Mo_2(O_2CR)_4]$ (**2**) (**2a**, R = CH_3; **2b**, R = $C(CH_3)_3$) with the H_2TMTAA ($C_{22}H_{24}N_4$) ligand in pentan-1-ol in the presence of DBU affords the new complexes $[Mo_2(TMTAA)(O_2CR)_2]$ (**1**) (**1a**, R = CH_3; **1b**, R = $C(CH_3)_3$). Complex **1a** has been structurally characterized. Crystal data for $[Mo_2(C_{22}H_{22}N_4)(O_2CCH_3)_2]$: triclinic, space group $P\bar{1}$, a = 8.801(5) Å, b = 11.572(8) Å, c = 13.714(9) Å, α = 108.42(6)°, β = 90.29(5)°, γ = 106.35(5)°, V = 1265(1) Å^3, Z = 2, D_c = 1.71 g·cm^{-3}, $F(000)$ = 824, μ(Mo Kα) = 10.06 cm^{-1}, and R = 0.039 (R_w = 0.034) for 410 parameters and 2973 unique data with $I > \sigma(I)$. The structure of **1a** consists of discrete dinuclear molecules in which the macrocyclic ligand has a very unusual bridging bis-bidentate coordination while the two acetato groups act as bridging ligands as in **2**. The two $[MoO_2N_2]$ moieties are in a quasi-perfectly eclipsed geometry, and the metal–metal bond length [2.106(1) Å] is in agreement with a $\sigma^2\pi^4\delta^2$ quadruple bond. SCF–MS–X_α calculations performed on a simplified C_{2v} model show that the δ(MoMo) orbital (HOMO) is definitely bonding and the δ^*(MoMo) orbital (LUMO) definitely antibonding with a significant HOMO/LUMO gap of 0.90 eV. The electrochemical behavior of complexes **1** was investigated. They are oxidizable in two one-electron reversible steps, leading successively to a stable mixed-valence $[Mo^{II}\overset{3.5}{-}Mo^{III}]^+$ compound and to a $[Mo^{III}\overset{3}{-}Mo^{III}]^{2+}$ species which decomposes readily. Two successive one-electron reduction steps lead to unstable $[Mo^{II}\overset{3.5}{-}Mo^{I}]^-$ and $[Mo^{I}\overset{3}{-}Mo^{I}]^{2-}$ derivatives. The electrochemistry of the $[\{Mo(TMTAA)\}_2]$ derivative **3** has been reexamined and compared to that of compounds **1** and **2**. The effect of the coordination mode of the macrocycle ligand on the electrochemical reactivity of the [Mo$\overset{4}{-}$Mo] core is discussed.

Introduction

Although superficially resembling a porphyrin, the 5,7,12,14-tetramethyldibenzo[*b*,*i*][1,4,8,11]tetraazacyclotetradecine macrocyclic ligand, H_2TMTAA ($C_{22}H_{24}N_4$; Figure 1), shows significant differences in electronic delocalization, core size, and framework flexibility.[2-4] These structural differences clearly induce differences in reactivity. This is well illustrated by their reaction with molybdenum hexacarbonyl: while H_2TMTAA (H_2L) affords a tetracarbonyl complex $[Mo(CO)_4(H_2L')]$ in which the N_4 macrocycle adopts very unusual behavior (neutral bidentate coordination with H transfer from a NH moiety to a CH unit),[5-7] H_2TPP gives rise to the quadruply metal–metal bonded molybdenum(II) complex $[\{Mo(TPP)\}_2]$ in which the porphyrin adopts its classical tetradentate dianionic form.[8] However, the TMTAA analog of this complex, i.e. $[\{Mo(TMTAA)\}_2]$ (**3**) (Figure 2), has been obtained by reaction of dimolybdenum tetraacetate, $[Mo_2(O_2CCH_3)_4]$, with the lithium salt Li_2TMTAA and fully characterized.[9,10]

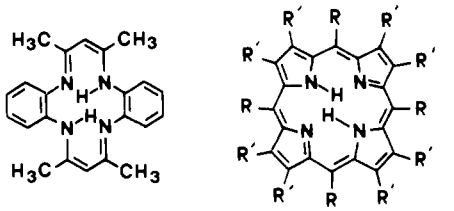

Figure 1. Comparison of N_4 macrocyclic ligands: Left, the 5,7,12,14-tetramethyldibenzo[*b*,*i*][1,4,8,11]tetraazacyclotetradecine macrocyclic ligand, H_2TMTAA ($C_{22}H_{24}N_4$); right, the porphyrin ligand. For H_2-TPP, R = C_6H_5 and R′ = H.

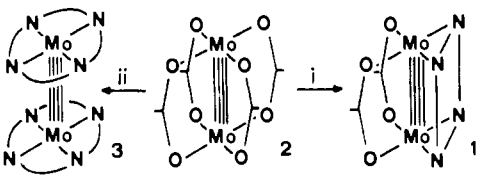

Figure 2. Syntheses of the molybdenum complexes from $[Mo_2(O_2CR)_4]$ (**2**). Key: (i) H_2TMTAA (H_2TMTAA/**2** = 2), pentan-1-ol, reflux in presence of DBU gives $[Mo_2(O_2CR)_2(TMTAA)]$ (**1**) (yield ca. 50%) (this work); (ii) Li_2TMTAA (Li_2TMTAA/**2** = 2), THF, −30 °C, gives $[\{Mo(TMTAA)\}_2]$ (**3**) (yield ca. 70%) (see ref 9).

(1) (a) URA CNRS 322. (b) URA CNRS 254. (c) URA CNRS 804.
(2) (a) Jager, E. G. *Z. Anorg. Allg. Chem.* **1969**, *364*, 177. (b) L'Epplatenier, F. A.; Pugin, A. *Helv. Chim. Acta* **1975**, *58*, 917. (c) Goedken, V. L.; Weiss, M. C. *Inorg. Synth.* **1980**, *20*, 115.
(3) Goedken, V. L.; Pluth, J. J.; Peng, S. M.; Bursten, B. *J. Am. Chem. Soc.* **1976**, *98*, 8014.
(4) For a recent review on mono- and dinuclear complexes of the H_2TMTAA ligand, see: Cotton, F. A.; Czuchajowska, J. *Polyhedron* **1990**, *9*, 2553.
(5) Bell, L. G.; Dabrowiak, J. C. *J. Chem. Soc., Chem. Commun.* **1975**, 512.
(6) Giraudon, J. M.; Mandon, D.; Sala-Pala, J.; Guerchais, J. E.; Kerbaol, J. M.; Le Mest, Y.; L'Haridon, P. *Inorg. Chem.* **1990**, *29*, 707.
(7) Cotton, F. A.; Czuchajowska, J. *Polyhedron* **1990**, *9*, 1217.
(8) Yang, C. H.; Dzugan, S. J.; Goedken, V. L. *J. Chem. Soc., Chem. Commun.* **1986**, 1313.
(9) Mandon, D.; Giraudon, J. M.; Toupet, L.; Sala-Pala, J.; Guerchais, J. E. *J. Am. Chem. Soc.* **1987**, *109*, 3490.
(10) Cotton, F. A.; Czuchajowska, J.; Feng, X. *Inorg. Chem.* **1990**, *29*, 4329.

0020-1669/93/1332-0713$04.00/0

In a continuation of our investigations on the ability of the H_2-TMTAA ligand to bind molybdenum ions, we have scrutinized the reaction between $[Mo_2(O_2CCH_3)_4]$ and the free macrocycle H_2TMTAA. For comparison, we have also examined the reaction of H_2TMTAA with $[Mo_2(O_2CC(CH_3)_3)_4]$, in which the very highly electron-donating *tert*-butyl group $C(CH_3)_3$ is present. As the analytical data for the resulting molybdenum(II) complexes **1** clearly showed an unusual TMTAA/metal ratio of 0.5, the solid-state molecular structure of the acetato complex was determined, to clearly establish the coordination mode of the N_4 ligand. Subsequently, this complex was further investigated by theoretical studies. The electrochemical behavior of these new compounds **1** was also investigated. The electrochemistry of the previously described $[\{Mo(TMTAA)\}_2]$ derivative **3**, shown in Figure 2, was reexamined more thoroughly in the present work in addition, since some misinterpretation was found in the previous work.[9] The electrochemistry of the tetracarboxylato derivatives $[Mo_2(O_2CR)_4]$[11,12] and of other $[Mo_2]$ derivatives with different ligands[13] has been previously described; the properties of the two $[Mo_2(O_2CR)_4]$ complexes with $R = CH_3$ and $R = C(CH_3)_3$ have been reexamined in details in the present experimental conditions. Together with the well-known tetracarboxylato derivatives $[Mo_2(O_2CR)_4]$, the $[Mo_2(TMTAA)(O_2CR)_2]$ and $[\{Mo(TMTAA)\}_2]$ derivatives constitute an interesting series to examine the effect of the coordination mode of the macrocyclic ligand on the electrochemical reactivity of the [Mo≡Mo] core; the results are discussed in the light of the MO diagram for these three kinds of compounds. Although some porphyrin complexes of the [Mo≡Mo] core[8,14] are known, their electrochemical properties have not yet been described; the "$Mo_2(TMTAA)_n$" complexes are thus the first examples of macrocyclic derivatives of the [Mo≡Mo] core whose electrochemistry is described.

Experimental Section

All reactions were performed in Schlenk tubes in a dry oxygen-free nitrogen atmosphere. Solvents were distilled by standard techniques and thoroughly deoxygenated before use. Elemental analyses were performed by "Service Central d'Analyse du CNRS-Vernaison, France".

IR spectra were recorded as KBr and CsI pellets with a Perkin-Elmer 1430 spectrophotometer. ESR spectra were obtained using a Jeol FE 3X spectrometer (X-band).

The apparatus, the three-compartment microelectrochemical cell, the treatment of the solvent, and the supporting electrolyte for the electrochemical studies have all been previously described.[15,16] The potentials are quoted versus the ferrocenium/ferrocene redox (Fc^+/Fc) system. For comparison of the present results with other works, the Fc^+/Fc formal potential has been measured versus SCE in benzonitrile (0.2 M, Bu_4NPF_6), $E'°(Fc^+/Fc) = +0.43$ V vs SCE.

Table I. Crystallographic Data for **1a**

chem formula	$C_{26}H_{28}Mo_2N_4O_4$	V, Å^3	1265(1)
fw	652.4	Z	2
space group	$P\bar{1}$	T, °C	23
a, Å[a]	8.801(5)	λ, Å	0.710 69
b, Å[a]	11.572(8)	ρ_{calcd}, g·cm^{-3}	1.71
c, Å[a]	13.714(9)	μ, cm^{-1}	10.06
α, deg[a]	108.42(6)	R[b]	0.039
β, deg[a]	90.29(5)	R_w[c]	0.034
γ, deg[a]	106.35(5)		

[a] From a least-squares fitting of the setting angle of 25 reflections. [b] $R = \sum||F_o| - |F_c||/\sum|F_o|$. [c] $R_w = [\sum_w||F_o| - |F_c||^2/\sum_w F_o^2]^{1/2}$, with $w = \{\sigma^2(I) + (0.04F_o^2)^2\}^{-1/2}$.

H_2TMTAA was prepared as previously described by Goedken and Weiss.[2c] Complexes $[Mo_2(O_2CR)_4]$ (**2**) were prepared according to the procedure of Stephenson et al. ($R = CH_3$) and McCarley et al. ($R = C(CH_3)_3$).[17]

Complex 1a. A mixture of $[Mo_2(O_2CCH_3)_4]$ (**2a**) (428 mg, 1 mmol) and H_2TMTAA (688 mg, 2 mmol) in pentan-1-ol (60 mL) was refluxed under dinitrogen for ca. 7 h in the presence of DBU (1,8-diazabicyclo-[5.4.0]undec-7-ene; $C_9H_{16}N_2$; 2 mL). The resulting solution was then slowly cooled to room temperature. The violet solid **1a** was filtered out, washed with pentane, and dried under reduced pressure (yield ca. 50%). Anal. Found: C, 47.1; H, 4.3; Mo, 29.9; N, 8.3. Calcd for $C_{26}H_{28}Mo_2N_4O_4$: C, 47.9; H, 4.3; Mo, 29.5; N, 8.6. IR data (cm^{-1}): 296 m, 335 s, 515 m, 625 m δ(OCO), 677 s δ(OCO), 745 s, 788 s, 832 m, 930 w, 1018 s, 1040 w, 1102 w, 1195 s, 1235 m, 1270 m, 1350–1550 br.

Complex 1b. **1b** was prepared from **2b** by a procedure similar to that described above for **1a** (yield ca. 50%). Anal. Found: C, 53.5; H, 5.7; Mo, 25.5; N, 7.8. Calcd for $C_{32}H_{40}Mo_2N_4O_4$: C, 52.2; H, 5.4; Mo, 26.1; N, 7.6. IR data (cm^{-1}): 425 m, 610 m, 690 w, 740 s, 755 w, 780 s, 830 m, 895 m, 930 m, 1015 m, 1100 w, 1150 w, 1190 s, 1220 s, 1270 m, 1355 s, 1370 s, 1410 vs, 1468 vs, 1482 s, 1504 s, 1545 vs.

Determination of the Crystal Structure of 1a. Data Collection. A violet crystal, ca. 0.20 × 0.15 × 0.20 mm, was sealed under dinitrogen in a capillary and placed on an Enraf-Nonius CAD-4 diffractometer, with graphite-monochromated Mo Kα radiation. All crystallographic data are given in Table I. Cell parameters were determined by least squares on setting angles from 25 reflections. Data were collected (ω–2θ scan; $t_{max} = 60$ s) in the following hkl range: h, 0 to 10; k, −13 to 13; l, −16 to 16 ($2\theta_{max} = 55°$). Intensity variation over the period of data collection: ±0.4%. A total of 4456 reflections were measured, 2973 unique with $I > \sigma(I)$ ($R_{int} = 0.016$). A Lorentz polarization correction was performed.

Determination and Refinement of the Structure. The structure was solved by Patterson and Fourier methods and refined by full-matrix least squares using anisotropic thermal factors for all non-hydrogen atoms while hydrogen atoms were refined isotropically. Refinement (2973 data, 410 parameters) was terminated with $R = 0.039$ and $R_w = 0.034$ [$w = \{\sigma^2(I) + (0.04F_o^2)^2\}^{-1/2}$]. The final difference map was flat [$|\Delta e|_{max} = 0.32$ e·Å^{-3}].

Atomic scattering factors were taken from ref 18. Calculations were performed on a Digital PDP 11/60 computer by using the SDP package of crystallographic program.[19]

Final atomic parameters are listed in Table II, and interatomic bond distances and angles in Table III.

Molecular Orbital Calculations. All the calculations have been made within the standard SCF–MS–X_α method.[20] The model **M** chosen for the calculations is a simplification of **1a**, in which the acetato ligands have been replaced by formato groups and TMTAA was replaced by the hypothetical $C_{10}H_{10}N_4$ ligand, using the same procedure as Cotton et al. in their theoretical study of $[\{Mo(TMTAA)\}_2]$.[10] This model is shown

(11) For a review, see: Casewitt, C. J.; Rakowski-Dubois, M. *Rev. Inorg. Chem.* **1988**, *9*, 199.
(12) (a) Cotton, F. A.; Pedersen, E. *Inorg. Chem.* **1975**, *14*, 399. (b) Santure, D. J.; Huffman, J. C.; Sattelberger, A. P. *Inorg. Chem.* **1985**, *24*, 371. (c) Cayton, R. H.; Chisholm, M. H.; Huffman, J. C.; Lobkovsky, E. B. *J. Am. Chem. Soc.* **1991**, *113*, 8709.
(13) (a) Cotton, F. A.; Frenz, B. A.; Pedersen, E.; Webb, T. R. *Inorg. Chem.* **1975**, *14*, 391. (b) Zietlow, T. C.; Hopkins, M. D.; Gray, H. B. *J. Am. Chem. Soc.* **1986**, *108*, 8266. (c) Zietlow, T. C.; Klendworth, D. D.; Nimry, T.; Salmon, D. J.; Walton, R. A. *Inorg. Chem.* **1981**, *20*, 947. (d) Coffindaffer, T. W.; Niccolai, G. P.; Powell, P.; Rothwell, I. P.; Huffman, J. C. *J. Am. Chem. Soc.* **1985**, *107*, 3572.
(14) (a) Tai, C. D.; Garner, J. M.; Collman, J. P.; Sattelberger, A. P.; Woodruff, W. H. *J. Am. Chem. Soc.* **1989**, *111*, 9072. (b) Collman, J. P.; Kim, K.; Garner, J. M. *J. Chem. Soc., Chem. Commun.* **1986**, 1711. (c) Collman, J. P.; Woo, L. K. *Proc. Natl. Acad. Sci. U.S.A.* **1984**, *81*, 2592.
(15) Le Mest, Y.; L'Her, M.; Courtot-Coupez, J.; Collman, J. P.; Evitt, E. R.; Bencosme, C. S. *J. Electroanal. Chem. Interfacial Electrochem.* **1985**, *184*, 331.
(16) Giraudon, J. M.; Sala-Pala, J.; Guerchais, J. E.; Le Mest, Y.; Toupet, L. *Inorg. Chem.* **1991**, *30*, 891; Err. **1991**, *30*, 3112.
(17) (a) Stephenson, T. A.; Bannister, E.; Wilkinson, G. *J. Chem. Soc.* **1964**, 2538. (b) McCarley, R. E.; Templeton, J. L.; Colburn, T. J.; Katovic, V.; Hoxmeier, R. J. *Adv. Chem. Ser.* **1976**, *No. 150*, 318.
(18) *International Tables for X-ray Crystallography*; Kynoch: Birmingham, England, 1974; Vol. IV.
(19) (a) Frenz, B. A. ENRAF-NONIUS Structure Determination Package; SDP Users guide, Version 1985. College Station, TX 77840 and ENRAF-NONIUS, Delft, The Netherlands. (b) Johnson, C. K. ORTEP. Report ORNL-3794, Oak Ridge National Laboratory, Oak Ridge, TN.
(20) (a) Slater, J. C. *Adv. Quantum Chem.* **1972**, *6*, 1. (b) Johnson, K. H. *Adv. Quantum Chem.* **1973**, *7*, 143. (c) Slater, J. C. *Quantum Theory of Molecules and Solids*; McGraw-Hill: New York, 1974; Vol. 4. (d) Johnson, K. H. *Annu. Rev. Phys. Chem.* **1975**, *26*, 39.

Table II. Final Fractional Atomic Coordinates in **1a**

atom	x	y	z	B,[a] Å^2
Mo1	−0.09759(5)	0.02454(4)	0.83188(3)	1.92(1)
Mo2	−0.10035(5)	0.01406(4)	0.67569(3)	1.92(1)
O1	−0.3440(4)	−0.0736(3)	0.8120(3)	2.65(8)
O2	−0.3479(4)	−0.0860(3)	0.6471(3)	2.64(8)
O3	−0.1509(4)	0.2005(3)	0.8765(3)	2.77(8)
O4	−0.1533(4)	0.1897(3)	0.7124(3)	2.74(8)
N1	−0.0366(5)	−0.1464(3)	0.8157(3)	2.07(9)
N2	−0.0409(5)	−0.1601(4)	0.6096(3)	2.26(9)
N3	0.1514(5)	0.1223(3)	0.8814(3)	2.13(9)
N4	0.1478(5)	0.1067(4)	0.6751(3)	2.22(9)
C1	0.4144(7)	0.1573(5)	0.9673(5)	3.8(1)
C2	0.2445(6)	0.0791(5)	0.9271(4)	2.4(1)
C3	0.1971(6)	−0.0441(5)	0.9369(4)	2.4(1)
C4	0.0796(6)	−0.1517(4)	0.8738(3)	2.1(1)
C5	0.0965(7)	−0.2784(5)	0.8715(4)	3.1(1)
C6	−0.1378(6)	−0.2576(4)	0.7402(4)	2.3(1)
C7	−0.1372(6)	−0.2663(4)	0.6357(4)	2.3(1)
C8	−0.2411(7)	−0.3727(5)	0.5623(4)	3.1(1)
C9	−0.3405(7)	−0.4697(5)	0.5905(5)	3.5(1)
C10	−0.3429(7)	−0.4600(5)	0.6925(5)	3.4(1)
C11	−0.2430(7)	−0.3530(5)	0.7676(4)	2.9(1)
C12	−0.4167(6)	−0.1104(5)	0.7229(4)	2.7(1)
C13	−0.5879(8)	−0.1864(7)	0.7042(5)	5.0(2)
C14	0.4095(7)	0.1346(6)	0.6078(5)	3.8(2)
C15	0.2397(6)	0.0609(5)	0.6088(4)	2.5(1)
C16	0.1918(6)	−0.0656(5)	0.5386(4)	2.7(1)
C17	0.0739(6)	−0.1710(4)	0.5482(4)	2.3(1)
C18	0.0921(7)	−0.3004(5)	0.4872(5)	3.4(1)
C19	0.2110(6)	0.2383(4)	0.8574(4)	2.5(1)
C20	0.2579(8)	0.3572(5)	0.9320(4)	3.4(1)
C21	0.3011(8)	0.4671(5)	0.9064(5)	4.1(2)
C22	0.2952(8)	0.4594(5)	0.8060(5)	3.9(1)
C23	0.2476(7)	0.3421(5)	0.7288(4)	3.2(1)
C24	0.2062(6)	0.2292(4)	0.7532(4)	2.4(1)
C25	−0.1634(6)	0.2482(5)	0.8063(4)	2.9(1)
C26	−0.187(1)	0.3750(6)	0.8333(5)	5.5(2)

[a] B values for anisotropically refined atoms are given in the form of the isotropic equivalent displacement parameter defined as $(4/3)[a^2B(1,1) + b^2B(2,2) + c^2B(3,3) + ab(\cos\gamma)B(1,2) + ac(\cos\beta)B(1,3) + bc(\cos\alpha)B(2,3)]$.

in Figure 3. The structural parameters of M were determined using the following procedure: Starting from the structure of **1a** determined by X-ray diffraction, the crystallographic coordinates were converted into a set of Cartesian coordinates. The origin of this Cartesian system was chosen to be the middle of the MoMo bond; the z axis was chosen to be colinear to the MoMo bond, and the x axis was chosen to be normal to a plane defined as the average between the least-squares planes of the four N atoms and the four O atoms. At this stage, the idealized C_{2v} symmetry was introduced by a coordinate averaging of the symmetry-related atoms. It was checked that the bond distances and angles of the model structure M are not significantly different from the corresponding averaged experimental values of **1a** (largest difference in bond distances: 0.0014 Å). All the C–H bond distances were set to 1.09 Å.

The muffin-tin atomic spheres were allowed to overlap. Due to the geometry, different reduction factors values for the atomic radii had to be considered, trying to keep an equilibrium between the electronic charge of the atomic spheres and their overlap, especially for the carbon atoms of the simplified TMTAA ligand. We used 90% of the atomic number radii for the core of the molecule (i.e. for Mo, O, N) and 82.5% for C. The hydrogen radius was fixed to 0.87 bohr, a value that has been computationally tested by us on several molecules. As usual, the outer sphere was taken close to the outermost atomic sphere, and its center was placed out of the MoMo axis, leading to the smallest possible intersphere region. The sphere radii are given in Table IV. The α parameters used (Table IV) are the α_{HF} of Schwarz,[21] except for hydrogen, where the Slater value[22] was chosen. Those relative to the outer-sphere (extramolecular) and the intersphere regions are weighted-average values of the atomic ones. Potential waves up to $l = 4$ were used for the outer sphere, up to $l = 2$ for the metal atoms, and up to $l = 1$ for O, C, and N. Only the $l = 0$ value was considered for H.

(21) (a) Schwarz, K. *Phys. Rev. B* **1972**, *5*, 2466. (b) Schwarz, K. *Theoret. Chim. Acta* **1974**, *34*, 225.
(22) Slater, J. C. *Int. J. Quantum Chem.* **1973**, *7*, 533.

Table III. Coordination Sphere of the Molybdenum Atoms in **1a**: Selected Bond Distances (Å) and Bond Angles (deg)[a]

Mo–Mo2	2.106(1)	Mo2–O2	2.127(4)
Mo1–O1	2.116(3)	Mo2–O4	2.119(4)
Mo1–O3	2.120(3)	Mo2–N2	2.145(4)
Mo1–N1	2.139(4)	Mo2–N4	2.146(4)
Mo1–N3	2.156(4)		
Mo2–Mo1–O1	91.4(1)	Mo1–Mo2–O2	91.62(9)
Mo2–Mo1–O3	92.0(1)	Mo1–Mo2–O4	90.93(9)
Mo2–Mo1–N1	98.1(1)	Mo1–Mo2–N2	100.0(1)
Mo2–Mo1–N3	99.4(1)	Mo1–Mo2–N4	98.5(1)
O1–Mo1–O3	89.6(1)	O2–Mo2–O4	90.0(1)
O1–Mo1–N1	91.8(2)	O2–Mo2–N2	91.3(2)
O1–Mo1–N3	169.1(1)	O2–Mo2–N4	169.8(1)
O3–Mo1–N1	169.8(1)	O4–Mo2–N2	168.9(1)
O3–Mo1–N3	90.9(2)	O4–Mo2–N4	91.5(2)
N1–Mo1–N3	85.8(2)	N2–Mo2–N4	85.3(2)

[a] Estimated standard deviations in the last significant figure are given in parentheses.

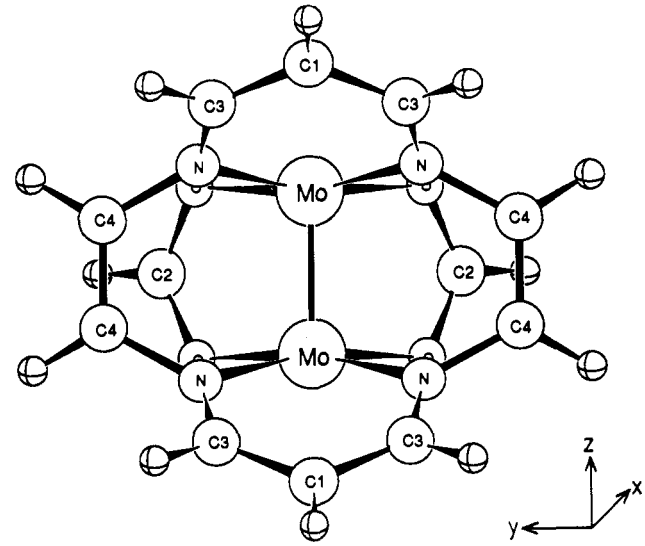

Figure 3. View of the model M used in the SCF–MS–X_α calculations. The atom labels refer to Table IV.

Table IV. SCF–MS–X_α Parameters Used in the Calculations

atom type[a]	α	radius (a_0)	atom type[a]	α	radius (a_0)
intersphere	0.759 73		C_1	0.759 28	1.6259
outer sphere	0.759 73	9.3325	C_2	0.759 28	1.4733
Mo	0.703 41	2.3426	C_3	0.759 28	1.5776
O	0.744 47	1.7567	C_4	0.759 28	1.6159
N	0.751 97	1.7217	H	0.777 25	0.8700

[a] See Figure 3.

Results and Discussion

Synthesis and IR Data. Treatment of dimolybdenum tetraacetate $[Mo_2(O_2CCH_3)_4]$ (**2a**) with 2 equiv of the 5,7,12,14-tetramethyldibenzo[1,4,8,11]tetraazacyclotetradecine ligand H_2-TMTAA ($C_{22}H_{24}N_4$; Figure 1) in pentan-1-ol at reflux in the presence of DBU (1,8-diazabicyclo[5.4.0]undec-7-ene; $C_9H_{16}N_2$) caused precipitation, after slow cooling to room temperature, of a violet solid **1a** in ca. 50% yield. IR spectroscopy clearly showed differences between **1a** and the previously reported dinuclear complex $[\{Mo(TMTAA)\}_2]$ (**3**), which we obtained from reaction of **2a** with the lithium derivative $[Li_2(TMTAA)]$.[9] A complete interpretation of the vibrational spectrum of **1a** was very difficult since superposition of various strong absorptions occurred in the 1350–1600-cm^{-1} region, giving a poorly resolved broad signal. If the presence of the macrocyclic ligand in **1a** was deduced from sharp characteristic absorptions at 745 and 1195 cm^{-1}, that of the acetato groups did not appear very clearly despite a careful comparison with the IR spectrum of the starting dinuclear complex

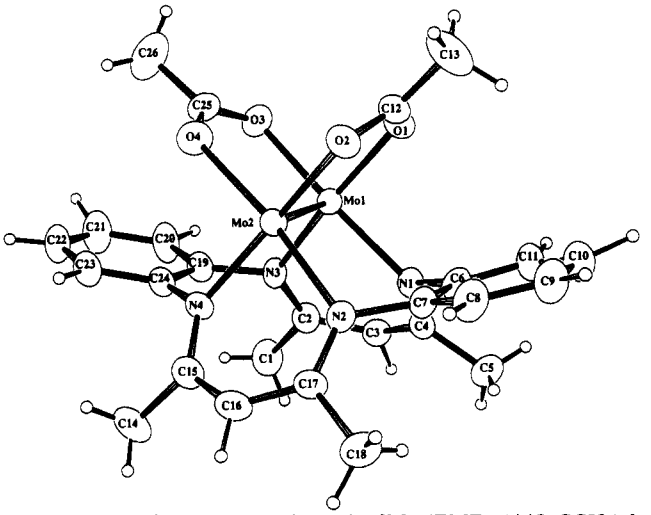

Figure 4. View of the structure of complex $[Mo_2(TMTAA)(O_2CCH_3)_2]$ (**1a**), showing the atom-labeling scheme. Hydrogen atoms are omitted for clarity. Non-hydrogen atoms are shown as 50% thermal ellipsoids.

$[Mo_2(O_2CCH_3)_4]$ (**2a**).[23] However, the presence of O_2CCH_3 groups, suggested by the absorption at 677 cm^{-1} attributable to δ(OCO) vibration,[23] was corroborated by elemental analyses which were in agreement with the formulation of **1a** as $[Mo_2(TMTAA)(O_2CR)_2]$ (R = CH_3). The analog **1b** with the highly electron-donating R = $C(CH_3)_3$ group was similarly obtained by reacting H_2TMTAA with the tetrapivalato complex $[Mo_2(O_2CR)_4]$ (**2b**, R = $C(CH_3)_3$).

Since H_2TMTAA usually gives 1/1 metal complexes,[4] the metal/macrocyclic ligand ratio observed in complexes **1** appeared extremely unusual, even though a similar value of two had been previously reported,[24,25] for example in rhodium chemistry for the $[Rh_2(TMTAA)(CO)_4]$ and $[Rh_2(HTMTAA)(CO)_4]ClO_4$ complexes.[24] It is noteworthy (i) that complexes **1** were prepared from reactions in which the starting Mo/H_2TMTAA ratio was one and not two and (ii) that all attempts to obtain $[\{Mo(TMTAA)\}_2]$ from reaction of $[Mo_2(O_2CR)_4]$ (**2**) with H_2-TMTAA failed, even when using a large excess of ligand, while displacement of all acetato ligands from **2a** easily occurred upon reaction with Li_2TMTAA.[9]

Structural Results. Figure 4 shows a perspective view of the molecule **1a** with the atomic numbering scheme. The structure consists of discrete dinuclear complex molecules with the macrocyclic ligand in a bridging bis-bidentate coordination mode, with each Mo(II) bonded to one of the 2,4-pentanediiminato chelate rings. The coordination around each molybdenum atom is completed by two bridging acetato groups cis to each other, the two MoO_2N_2 fragments being in a quasi-perfectly eclipsed geometry. The maximum point symmetry permitted with this ligand arrangement is C_{2v}, and the dinuclear molecule has virtually this symmetry. Therefore, complex **1a** has a structure which shows important analogies with that of the starting dinuclear acetato complex **2a**. For example, from a structural point of view, formation of **1** from **2** may formally appear as a simple substitution of two bridging carboxylato groups by the bis-bridging dianionic TMTAA ligand without significant structural changes

Table V. Comparison of Average Dihedral Angles[a] (deg) and Selected Average Interatomic Distances (Å) in [Mo(TMTAA)] Complexes[b]

	bis-bident TMTAA	tetradent TMTAA	
	1[c]	**4**[d]	**5**[e]
1–2 angle(av)[a]	48.9(2)	32.2	33.8
1–3 angle(av)[a]	9.2(8)	13.9	
1–4 angle(av)[a]	13.6(4)	21.4	22.5
dist of Mo from N_4 plane	1.540(1)	0.570(5)	0.737(1)
Mo–N dist			
from	2.139(4)	2.057(4)	2.034(4)
to	2.156(4)	2.079(4)	2.041(4)
av	2.146(4)	2.068(4)	2.038(4)

[a] See definition of dihedral angles in Figure 5. [b] Similar data for TMTAA complexes with other metals are given in ref 29. [c] **1**, $[Mo_2(O_2CCH_3)_2(TMTAA)]$; this work. [d] **4**, $[\{Mo(TMTAA)\}_2]PF_6$; see ref 9. [e] **5**, $[MoO(TMTAA)][C_3(CN)_5]$; see ref 16.

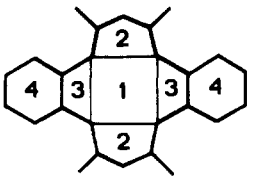

Figure 5. Definition of molecular planes. The dihedral angles for **1a** and other [Mo(TMTAA)] complexes are given in Table V.

and particularly without significant modification in the metal–metal bond length. As in **2** (MoMo = 2.0934(8) Å),[26] the metal–metal bond length in **1a** (2.106(1) Å) is in agreement with a $\sigma^2\pi^4\delta^2$ quadruple bond.[27]

The structure of complex **1a** may be also roughly compared to that of the previously described $[Rh_2(TMTAA)(CO)_4]$ complex, with the two bridging acetato groups taking the place of the four terminal carbonyl ligands.[24] However, and as expected, these two complexes strongly differ in the nature of the metal–metal interaction since only a weak bonding interaction (RhRh = 3.086 Å) was observed in the rhodium derivative.[24]

The macrocyclic ligand displays a geometry which corresponds to a significant deformation from its usually stable saddle shape.[3,4] The four nitrogen atoms are coplanar within 0.004 Å, and the Mo_2 fragment is parallel to this plane (Mo–N_4 mean plane distances: 1.539(1) and 1.541(1) Å). It is noteworthy that these displacements are much greater than those observed in $[\{Mo(TMTAA)\}_2]PF_6$ (**4**) (0.570(5) Å)[9] and $[MoO(TMTAA)][C_3(CN)_5]$ (**5**) (0.737(1) Å),[16] in which the macrocyclic ligand shows its usual tetradentate coordination mode (Table V). The average Mo–N bond length in **1a** (2.146(4) Å) is considerably longer than the averages of 2.068(4) and 2.038(4) Å found in **4** and **5**, respectively.

It is of prime interest to note that in going from the tetradentate to the bis-bidentate coordination mode, the most significant change in the geometry of the ligand corresponds to a significant twisting about the C–N bonds of the 2,4-pentanediiminato chelate rings, the angle between these two rings increasing from ca. 65° to ca. 98° (Table V). On the other hand, the average angle between the two benzene rings decreases from ca. 44° in **4** and **5** to ca. 27° in **1**.

As in other complexes of the TMTAA ligand,[3,4,9,16] the four CN bonds of the *o*-phenylenediamine residues (average length 1.431(6) Å) have predominant single-bond character and break the electronic delocalization that is primarily limited to the benzene rings and the NCCCN units.

(23) Clark, R. J. H.; Hempleman, A. J.; Kurmoo, M. *J. Chem. Soc., Dalton Trans.* **1988**, 973 and references therein.
(24) Gordon, G. C.; DeHaven, P. W.; Weiss, M. C.; Goedken, V. L. *J. Am. Chem. Soc.* **1978**, *100*, 1003.
(25) Other examples of H_2TMTAA complexes having a M/TMTAA ratio equal to two have been also reported. (a) $[\{Re(CO)_3\}_2(TMTAA)]$ has been briefly described by: Kadish, K. M.; Bottomley, L. A.; Schaeper, D.; Tsutsui, M.; Bobsein, R. L. *Inorg. Chim. Acta* **1979**, *36*, 219. (b) $[Ru_2(HTMTAA)(PhCCPh)(O_2CCH_3)_3]$ has been obtained by: Cotton, F. A.; Czuchajowska, J. (*J. Am. Chem. Soc.* **1991**, *113*, 3427) from reaction of $[Ru_2(O_2CCH_3)_4]$ with H_2TMTAA in presence of PhCCPh. Actually, the crystal structure study of this complex revealed a coupling reaction between the HTMTAA and PhCCPh fragments.
(26) Cotton, F. A.; Mester, Z. C.; Webb, T. R. *Acta Crystallogr., Sect. B* **1974**, *B30*, 2768.
(27) (a) Cotton, F. A.; Curtis, N. F.; Harris, C. B.; Johnson, B. F. G.; Lippard, S. J.; Mague, J. T.; Robinson, W. R.; Wood, J. S. *Science* **1964**, *145*, 1305. (b) Cotton, F. A. *Inorg. Chem.* **1965**, *4*, 334.

Table VI. Valence Molecular Orbital Data for the C_{2v} Model M of **1a**

			% charge						Mo angular contribn		
	levels	*E*, eV	int.	out.	Mo_2	$(acet)_2$	tmtaa		% s	% p	% d
	$17b_1$	−3.296	69	10	19	1	1	σ^*(Mo–Mo)		11	89
	$17b_2$	−3.677	47	6	32	8	8				100
	$16b_1$	−3.812	59	6	5	0	30				
	$14a_2$	−3.934	20	1	35	5	39				100
	$16b_2$	−4.541	39	2	2	0	57				
	$13a_2$	−4.700	26	0	27	0	46			1	99
	$15b_1$	−4.988	17	0	76	1	6	π_σ^*(Mo–Mo)		1	99
	$12a_2$	−5.233	22	0	53	2	23	π^*(Mo–Mo)			100
LUMO	$14b_1$	−6.371	11	0	75	6	7	δ^*(Mo–Mo)			100
HOMO	$19a_1$	−7.270	19	0	48	3	30	δ(Mo–Mo)			100
	$18a_1$	−7.927	25	0	32	1	41		1	1	98
	$13b_1$	−8.341	30	0	5	2	63				
	$15b_2$	−8.552	27	0	14	6	53			7	93
	$17a_1$	−9.208	31	0	12	3	53		18	3	79
	$16a_1$	−9.424	20	0	32	40	7		12	3	85
	$14b_2$	−9.523	17	0	54	15	14	π(Mo–Mo)			100
	$15a_1$	−9.678	17	0	62	14	6	π_σ(Mo–Mo)	2	3	95
	$11a_2$	−10.11	17	0	1	42	39				
	$13b_2$	−10.13	23	1	17	36	23			9	91
	$12b_1$	−10.44	16	0	3	71	10				
	$10a_2$	−10.51	17	0	0	75	7				
	$14a_1$	−10.75	13	0	53	14	20	σ(Mo–Mo)	6	4	90

The $[Mo_2(O_2CCH_3)_2]$ fragment reveals no unexpected features and contains almost perpendicular acetato groups. It is noteworthy that the Mo–O bond distances, ranging from 2.226(3) to 2.127(4) Å, are comparable to those observed in other $[Mo_2(\mu$-acetato$)_n]$ complexes.[28]

Theoretical Analysis. SCF–MS–X_α calculations have been performed on a simplified C_{2v} model of complex **1**, namely **M**, shown in Figure 3. The way the structure of this complex has been set up, and the calculations have been carried out, is discussed in the Experimental Section. The energy, symmetry, and charge distribution of the highest occupied and lowest unoccupied molecular levels are given in Table VI.

Under the C_{2v} symmetry of the molecule, the σ (d_{z^2}) and δ ($d_{x^2-y^2}$) metallic orbitals belong to the same a_1 irreducible representation, as does one component of the π orbitals (d_{xz}) that we shall name π_σ. Therefore, these δ, σ, and π_σ orbitals are allowed to mix in the complex. However, this mixing is not important, due to the strong 4-fold pseudosymmetry around the metal atoms. Although the metallic levels can also mix with ligand levels of the same symmetry, which lie close in energy, it is possible to identify unambiguously the bonding and antibonding orbitals which can be associated with the σ, δ, π_σ, and π MoMo bonds (Table VI). This is illustrated in Figure 6, which shows plots of all the metal–metal bonding combinations and of the δ^* antibonding orbital. From these data it appears that the δ(MoMo) orbital (which is the HOMO of **M**) is definitely bonding and that the δ^*(MoMo) orbital (which is the LUMO) is definitely antibonding. In accord, the HOMO/LUMO gap is significant (0.90 eV). It is clear that a quadruple bond is present in this molecule, a finding which agrees with the observation of a short MoMo distance in **1a** (2.106(1) Å).

It is interesting to compare our theoretical results with those obtained by the same method of calculation on related complexes containing MoMo quadruple bonds.[30] Cotton et al.[10] have carried out X_α calculations on a model for $[\{Mo(TMTAA)\}_2]$ (**3**), in which each Mo atom is bonded to the four nitrogen atoms of the same TMTAA ligand. Although the occupied MoMo δ orbital of this complex appears significantly bonding, the HOMO/LUMO gap (0.38 eV) is about half the one we found on **1**. This result suggests that the δ bond in **1** is stronger than that in **3**, consistent with the fact that the MoMo bond distance in $[\{Mo(TMTAA)\}_2]$ is longer[10] (2.22 Å vs 2.11 Å).

Norman et al.[31] have carried out X_α calculations on $[Mo_2(O_2CH)_4]$, in which each formato ligand is bonded to both Mo atoms. The HOMO/LUMO gap they calculated is large (1.51 eV), indicating the presence of a strong δ bond.[32] This is consistent with the fact that the MoMo distance in this complex is particularly short (2.09 Å).[33] A comparison of the calculations on the three complexes leads to the conclusion that carboxylato ligands favor the formation of a strong MoMo quadruple bond, as found for $[Mo_2(O_2CH)_4]$,[31] while with the more covalent TMTAA ligand the metal–metal bonding interactions compete with the metal–ligand one. Compound **1**, which contains the two types of ligands, appears to be intermediate between these two situations. This ligand effect can be attributed to the difference in the π-donating ability of the ligands. The δ frontier orbital of each ML_4 "monomeric" subunit affords some destabilization arising from interaction with a π-type ligand orbital of the same local symmetry. This destabilization of the Mo δ frontier orbital will induce a similar destabilization of their bonding combination in the "dimer" and therefore reduce the HOMO/LUMO gap of the dinuclear complex. In addition, the mixing of the "monomeric" δ frontier orbital with the π-type ligand lowers the metallic character of the δ frontier orbital. The larger the mixing, the lower the overlap between two δ "monomeric" orbitals and consequently the weaker the MoMo δ bond in the "dimer". Oxygen atoms are weak π-donors; therefore carboxylato ligands will favor larger HOMO/LUMO gaps and stronger δ bonds. In contrast, nitrogen ligands such as TMTAA, which are better π-donors, will favor smaller HOMO/LUMO gaps and weaker δ bonds.

Finally, it is interesting to note a typical feature found in the three calculations: the δ^* LUMO is separated from the other vacant orbitals by a gap larger than 1 eV. Consequently, in our calculations as in those of Norman et al.,[31] this level is situated in the middle of a large gap separating the HOMO from the second lowest vacant orbital.

(28) Cotton, F. A.; Isley, W. H.; Kaim, W. *Inorg. Chem.* **1981**, *20*, 930 and references therein.
(29) Tsutsui, M.; Bobsein, R. L.; Cash, G.; Pettersen, R. *Inorg. Chem.* **1979**, *18*, 758 and references therein.
(30) For a recent and general discussion on the theoretical aspects of the metal–metal quadruple bond, see: Wiest, R.; Strich, A.; Bénard, M. *New J. Chem.* **1991**, *15*, 801 and references therein. See also: Losada, J.; Alvarez, S.; Novoa, J. J.; Mota, F.; Hoffmann, R.; Silvestre, J. *J. Am. Chem. Soc.* **1990**, *112*, 8998.
(31) Norman, J. G., Jr.; Kolari, H. J.; Gray, H. B.; Trogler, W. C. *Inorg. Chem.* **1977**, *16*, 987.
(32) An ab initio study on $[Mo_2(O_2CH)_4]$ has also been published: Atha, P. M.; Hillier, I. H.; Guest, M. F. *Mol. Phys.* **1982**, *46*, 437.
(33) Cotton, F. A.; Norman, J. G., Jr.; Stults, B. R.; Webb, T. R. *J. Coord. Chem.* **1976**, *5*, 217.

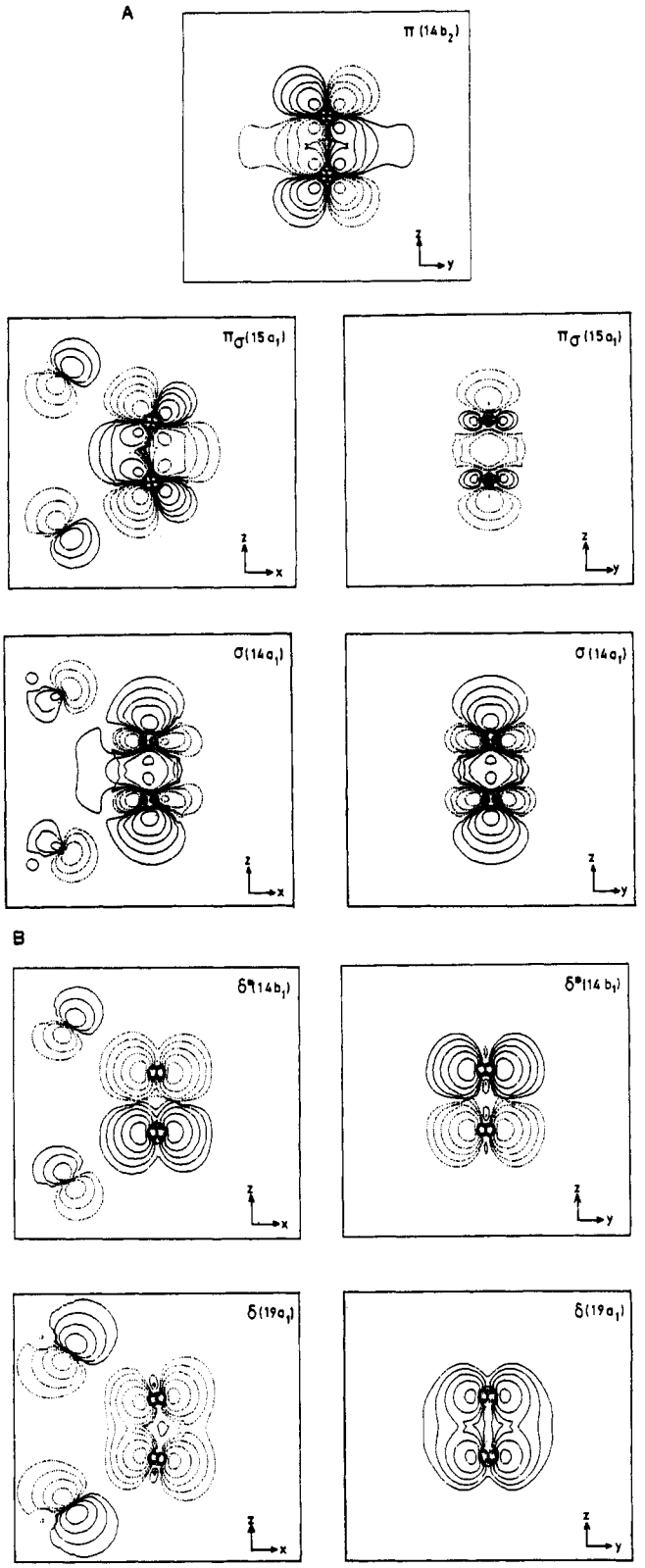

Figure 6. Contour map of the metallic MO's in the *xz* and *yz* planes (contour values ±0.01, ±0.02, ±0.04, ±0.08, ±0.16): (A) σ(MoMo), π(MoMo), π_σ(MoMo); (B) δ(MoMo), δ^*(MoMo).

Electrochemistry. A comparative picture of the electrochemical behavior of the three types of complexes, $[Mo_2(TMTAA)(O_2CR)_2]$ (**1**), $[Mo_2(O_2CR)_4]$ (**2**), and $[\{Mo(TMTAA)\}_2]$ (**3**) is presented in Figure 7, in the case of R = CH_3, and the electrochemical data are presented in Table VII.

$[Mo_2(TMTAA)(O_2CR)_2]$ (1). In PhCN, the pivalate derivative **1b** gave the same response as the acetate **1a**; the study was developed with the acetate derivative due to the low stability of

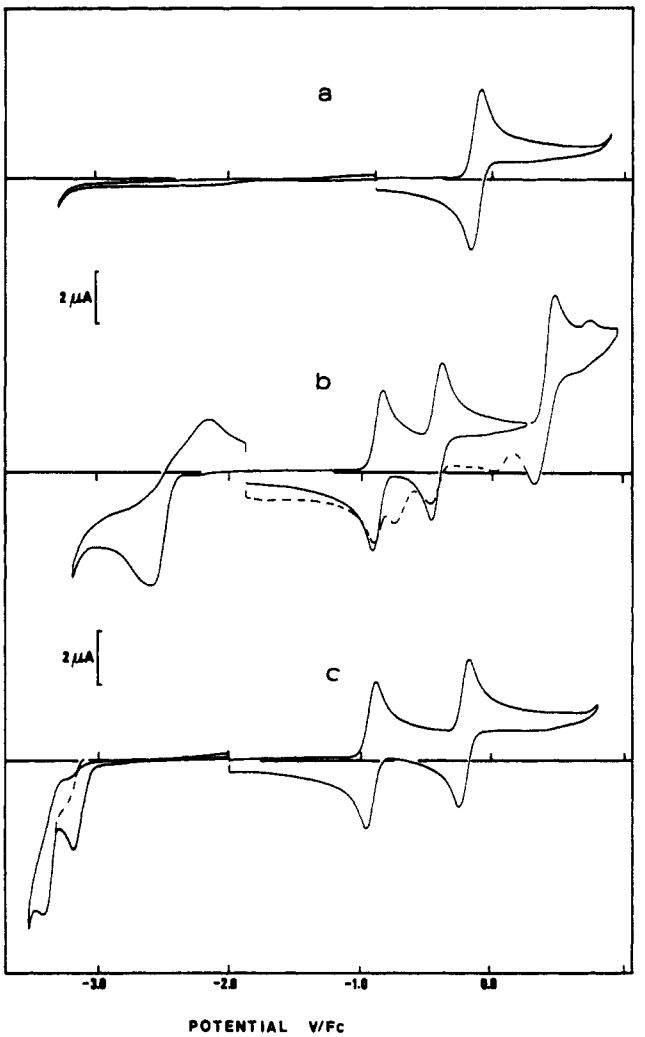

Figure 7. Cyclic voltammetry of (a) $[Mo_2(O_2CCH_3)_4]$ (**2a**), (b) $[\{Mo(TMTAA)\}_2]$ (**3**), and (c) $[Mo_2(TMTAA)(O_2CCH_3)_2]$ (**1a**), in THF containing 0.2 M Bu_4NPF_6. Key: *C* ca. 10^{-3} M; platinum disk electrode; scan rate 100 mV/s; reference Fc^+/Fc.

the pivalate compound. As shown on the typical voltammogram in Figure 7, curve c, both compounds, with R = CH_3 or $C(CH_3)_3$, display in the electrochemical range of PhCN, THF, and CH_2Cl_2, two reversible redox processes followed by a totally irreversible peak (not shown in the figure). These first two processes have cyclic voltammetry (CV) characteristics indicative of one electron diffusion-controlled reversible exchanges for scan rate v, $0.01 < v < 1$ V/s (i.e. $\Delta E_p \simeq 60$ mV, $i_{pa}/i_{pc} \simeq 1$, and $i_p/v^{1/2}$ is constant); they correspond to two oxidation waves with equal height at a rotating disk electrode (RDE). In the reduction range, two partially reversible systems can be seen at a potential very close to the THF reduction limit. The two cathodic peaks of these systems have exactly the same height and shape as those of the two first oxidation processes. They display a reoxidation anodic peak which can only be distinctly seen for scan rate, v, more than 0.1 V/s and whose intensity increases with v. Owing to the very low value of the potentials of these systems, it can be deduced that the reduced forms of the complexes are very reactive and have a very short lifetime.

Bulk electrolysis of a solution of $[Mo_2(TMTAA)(O_2CR)_2]$ at a potential more positive than the first process generates, after an exchange of $n = 0.9 \pm 0.1$ electron per molecule, a solution whose CV is the same as the initial one over a few hours, reflecting the stability of the one-electron oxidized species. Conversely, the product obtained through the second one-electron oxidation process is not stable on the electrolysis time scale. This is indicated by the degradation of the CV after bulk electrolysis. The

Table VII. Electrochemical Data for the MoMo Complexes: E'°/V^a (ΔE_p/mV)[b]

complex	solvent	redn steps		oxidn steps		
		E'°_5 (ΔE_p)	E'°_4 (ΔE_p)	E'°_1 (ΔE_p)	E'°_2 (ΔE_p)	E'°_3 (ΔE_p)
$[Mo_2(O_2CR)_4]$						
R = CH_3	PhCN			–0.01 (70)		
	CH_2Cl_2			0.12 (80)		
	THF			–0.12 (80)		
R = $C(CH_3)_3$	PhCN			–0.02 (70)		
	CH_2Cl_2			0.12 (80)		
	THF			–0.12 (80)		
$[Mo_2(TMTAA)(O_2CR)_2]$						
R = CH_3	PhCN			–0.73 (60)	–0.01 (60)	E_{pa} = +1.38 (irr)
	CH_2Cl_2			–0.62 (80)	0.06 (80)	
	THF	–3.32 (180)	–3.10 (100)	–0.82 (80)	–0.10 (80)	
R = $C(CH_3)_3$	PhCN			–0.74 (60)	–0.02 (60)	E_{pa} = +1.38 (irr)
	CH_2Cl_2			–0.66 (80)	0.02 (80)	
	THF	–3.38 (140)	–3.16 (120)	–0.86 (80)	–0.14 (110)	
$[\{Mo(TMTAA)\}_2]$						
	PhCN			–0.84 (70)	–0.40 (70)	0.44 (110)[c]
	CH_2Cl_2			–0.96 (70)	–0.44 (70)	E_{pa} = 0.48
	THF		E_{pc} = –2.55 (300)	–0.88 (80)	–0.42 (80)	0.40 (120)[c]

[a] Obtained from cyclic voltammetry in solvents + Bu_4NPF_6 (0.2 M); Pt disk; 100 mV/s; E'° versus Fc^+/Fc reference electrode. [b] $\Delta E_p = E_{pa} - E_{pc}$. [c] Separation between the two main peaks.

coulometric value is typically $n = 1.8 \pm 0.3$ electrons per molecule, when the electrolysis is interrupted at a current level a tenth to a twentieth of the initial one. A very long exhaustive electrolysis leads to a total degradation of the solution. Among the new peaks observed in the CV after electrolysis the most prominent ones correspond to pseudoreversible processes located at ca. 0.40, –0.72, and –2.22 V. These are typical of a $[MoO(TMTAA)]^+$ derivative,[16] a species whose presence is also indicated by the appearance of its ESR spectrum (vide infra). Similar observations could also be made when electrolysis was performed at a potential corresponding to the first oxidation over a long period of time at a current level close to the background. The source of oxygen in the formation of the oxo species is probably the residual water in the solvent although in very low concentration. Bulk electrolyses performed at potentials more cathodic than the two reduction peaks failed to produce any result other than totally decomposed solutions. Attempts to chemically (NaHg) reduce the complexes **1** also failed.

$[\{Mo(TMTAA)\}_2]$ (3). We have previously described briefly the electrochemical behavior of $[\{Mo(TMTAA)\}_2]$;[9] for comparison, it was reexamined here. Moreover, a misinterpretation in the assignment of the redox processes was found in the earlier work.[9] As shown in Figure 7b, $[\{Mo(TMTAA)\}_2]$ gives rise to two fully reversible processes, at –0.84 and –0.40 V in PhCN, followed by a third more complex one. The latter oxidation process displays two anodic peaks associated with a large cathodic peak and two smaller cathodic peaks shown by the dashed line in the figure, one of them at a much more negative potential, ca. –0.7 V. In THF, a reduction process is observed at –2.55 V; the height of the cathodic peak is a little less than twice that of the two reversible peaks; the anodic peak of this system is very broad with ΔE_P = 340 mV. At a rotating disk electrode, a solution of the neutral $[\{Mo(TMTAA)\}_2]$ compound shows *two successive oxidation waves* of equal heights, corresponding to the first two reversible processes, and not *one reduction and one oxidation wave* as previously reported.[9] These are followed by a more complex composite wave, corresponding to the third oxidation process, whose height equals that of the sum of the first two. The same height was found for the RDE wave of the cathodic process.

Bulk electrolysis performed on the complexes in PhCN, at a potential more anodic than the first waves, gave coulometric values equal to $n = 0.9 \pm 0.1$ faraday/mol. The oxidation product of the first process has the same electrochemical characteristics as the starting material, indicating an uncomplicated oxidation process. Conversely, after oxidation at a potential more anodic than the second wave, as is observed in the case of the $[Mo_2(TMTAA)(O_2CR)_2]$ complex, the RDE and cyclic voltammograms indicate the formation of a mixture of $[\{Mo(TMTAA)\}_2]^{2+}$ and $[MoO(TMTAA)]^+$.[16] No electrolysis was performed at the potential of the third oxidation process. However, the CV is indicative of a coupled chemical reaction through the presence of several cathodic peaks associated with the anodic peak and with a decrease of those of the starting material, while peaks characteristic of $[MoO(TMTAA)]^+$ appear when the potential sweep is interrupted during a few minutes at a potential more anodic than that process. Every attempt to generate a reduced species, at potentials more cathodic than each of the two reduction waves, failed and gave decomposition products.

$[Mo_2(O_2CR)_4]$ (2). For the purpose of comparison, the electrochemical behavior of the tetracarboxylato complexes $[Mo_2(O_2CR)_4]$ with R = CH_3 (Figure 7a) or $C(CH_3)_3$, although previously briefly described,[12] was reexamined. Contrary to what was previously anticipated, these derivatives are soluble enough to allow electrochemical and ESR studies; the pivalate complex is more soluble but is less stable in solution. These derivatives give rise to an oxidation process whose cyclic voltammetry (CV) characteristics are indicative of a one-electron diffusion-controlled reversible exchange; this first process is followed by a totally irreversible wave close to the solvent discharge. Down to –3.5 V vs the Fc^+/Fc electrode in THF, no reduction system is observed. Exhaustive electrolysis of the solutions, at a potential corresponding to the first oxidation wave, indicated coulometric values of $n = 1.0 \pm 0.1$ faraday/mol and generated solutions of the oxidized species stable over a few hours, sufficient for ESR characterization.

ESR. A set of spectra recorded at room and low temperature (130 K) in PhCN is presented in Figure 8 for the three kinds of compounds with R = CH_3, oxidized at a potential corresponding to the first oxidation wave. Data are reported in Table VIII. The ESR spectra of the reduced solutions of $[Mo_2(TMTAA)(O_2CR)_2]$ and $[\{Mo(TMTAA)\}_2]$ were noninterpretable, with very low intensity.

$[Mo_2(TMTAA)(O_2CR)_2]$ (1). The isotropic room temperature spectra of the two carboxylato derivatives, **1a,b**, after oxidation at a potential corresponding to the first wave, show the usual pattern of three components of one, six, and eleven lines, as expected for a delocalized electron on two equivalent molybdenum nuclei ($^{92,94,96,98,100}Mo$, $I = 0$, natural abundance ca. 75%; $^{95,97}Mo$, $I = {}^5/_2$, natural abundance ca. 25%).[11,12a,13a] The low-temperature spectra show very poor resolution, and it was not possible to determine whether they correspond to a delocalized

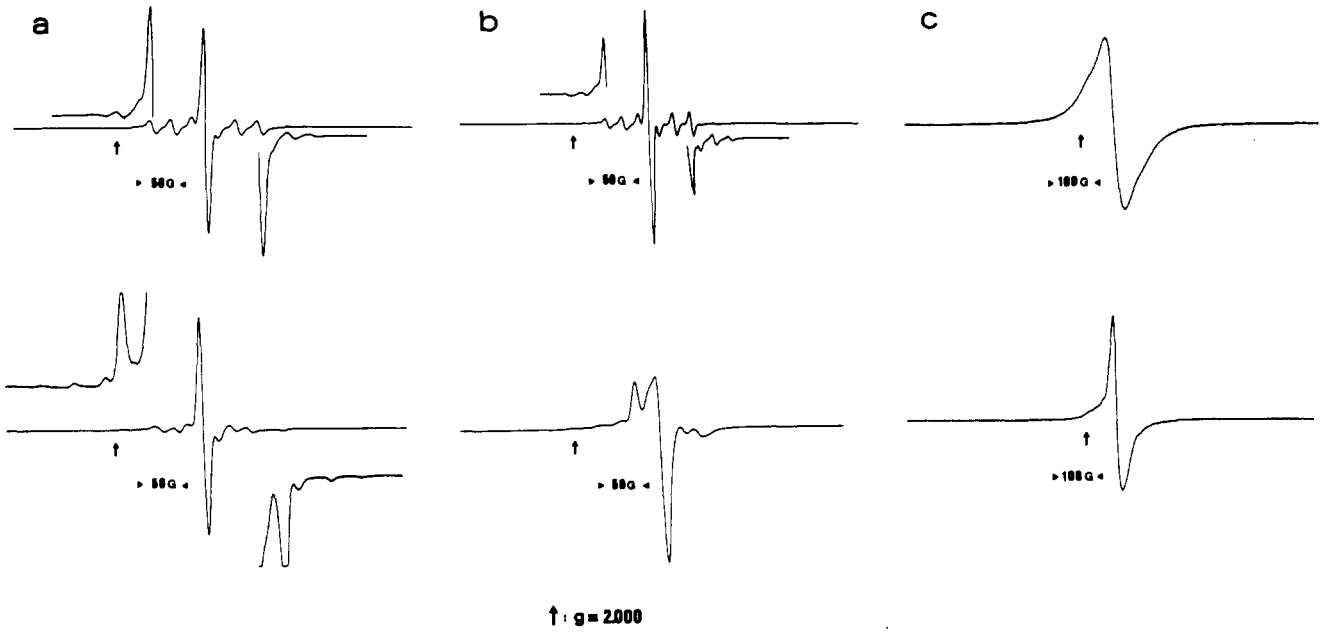

Figure 8. ESR spectra of the molybdenum complexes in benzonitrile after electrolyses at potentials more anodic than the first oxidation waves: Upper part, room temperature (298 K); lower part, low temperature (130 K). Key: (a) $[Mo_2(O_2CCH_3)_4]$ (**2a**); (b) $[Mo_2(TMTAA)(O_2CCH_3)_2]$ (**1a**); (c) $[\{Mo(TMTAA)\}_2]$ (**3**).

Table VIII. ESR Data for the Oxidized Forms of the MoMo Complexes[a]

complex	g_{iso}	A_{iso}	$g_\parallel$	$g_\perp$	$A_\parallel$
$[Mo_2(O_2CCH_3)_4]^+$	1.932	28	1.933	1.933	41
$[Mo_2(O_2CC(CH_3)_3)_4]^+$	1.933	26		1.934[b]	40
$[Mo_2(TMTAA)(O_2CCH_3)_2]^+$	1.941	22	1.958[c]	1.936[b]	
$[Mo_2(TMTAA)(O_2CC(CH_3)_3)_2]^+$	1.942	22	1.955[c]	1.937[b]	
$[\{Mo(TMTAA)\}_2]^+$	1.954			1.956[b]	

[a] In PhCN, 0.2 M Bu_4NPF_6; C ca. 10^{-3} M. A in gauss throughout this paper, 1 G = 10^{-4} T; 298 K for the room-temperature spectra and 130 K for the low-temperature spectra. [b] Central line. [c] Most intense low-field line.

mixed-valence form in a frozen solution. These spectra appear to be composed of a central line and a less intense left-hand line, tentatively referred respectively as $g_\perp$ and $g_\parallel$ in Table VIII; moderately intense lines on the right-hand side of the spectra could however be assigned to the third component of a rhombic spectrum. This shape seems to indicate a rhombic geometry is more likely than the axial arrangement observed for the tetracarboxylato derivatives (vide infra).

Contrary to expectation, the solutions oxidized at a potential more anodic than the second reversible process are not ESR silent. During the oxidation the intensity of the initial signal of $[Mo_2(TMTAA)(O_2CR)_2]^+$ decreases, while a new signal appears and increases in intensity. The characteristics of this signal at room temperature, g_{iso} = 1.958 and A_{iso} = 35 G, as well as the low-temperature spectrum, are those of the previously described $[MoO(TMTAA)]^+$ derivative.[16] The latter signal becomes the only one observable when the electrolysis is continued exhaustively. This corroborates the results of the electrochemistry. No other signal could be observed at any time during the electrolysis, indicating that the oxidized form, $[Mo_2(TMTAA)(O_2CR)_2]^{2+}$, detected by RDE voltammetry, is ESR silent, as expected.

$[\{Mo(TMTAA)\}_2]$ (3). The product of the first one-electron oxidation process displays ESR spectra which are very broad both at room and low temperature, as shown in Figure 8c; they do not show any resolved coupling. This is probably due to the very large value of the line width (central line line width ca. 53 G), precluding any resolution of the satellite lines which should have coupling constants in the range of 20–60 G. In the room-temperature spectrum, deformations on each side of the central line are ascribable to the six-line set, while those corresponding to the putative eleven-line set for a delocalized mixed-valence $[Mo_1^{II\,3.5}—Mo_2^{III}]^+$ derivative, with $I_{Mo1} = I_{Mo2} = {}^5/_2$, cannot be distinguished from the base line. Although the low-temperature spectrum could not be resolved (Figure 8c) its shape is consistent with an axial geometry; cf. the tetracarboxylato derivatives. As for the other TMTAA derivatives **1**, the solution resulting from the second oxidation is not ESR silent but only displays the typical ESR signal of $[MoO(TMTAA)]^+$, both at room and low temperature (vide supra).

$[Mo_2(O_2CR)_4]$ (2). The spectra obtained for both compounds, with R = CH_3 and R = $C(CH_3)_3$, after oxidation at a potential corresponding to the first wave, are very similar, as previously described.[11,12b,17b,34] The low-temperature spectra are also similar to that of the derivative with R = C_3H_7.[12a] They all display symmetric character with regard to the central line and are interpreted as an axial spectrum with g values of the perpendicular and parallel components nearly equal. This interpretation reflects the axial geometry of the complexes. As expected for a delocalized mixed-valence $[Mo^{II\,3.5}—Mo^{III}]^+$ compound, the three sets of 1, 6, and 11 lines are observed on the parallel component of the spectra. In the case of the present compounds, the isotropic room-temperature spectra could also be obtained, and in these the three sets of lines are also observable and the eleven-line set is clearly distinguishable, as shown in Figure 8a.

Comments on the Electrochemical Reactivity of the [Mo⁴—Mo] Quadruple Bond. The present results exemplify the electrochemical reactivity of the dimolybdenum quadruple bond, which can be summarized by the following scheme:

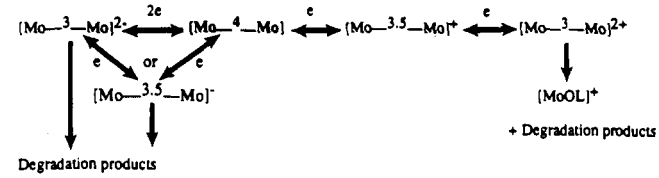

The $[Mo^{II\,4}—Mo^{II}]$ core can be oxidized in two reversible one-electron steps. The first step leads to stable mixed-valence $[Mo^{II\,3.5}—Mo^{III}]^+$ class III compounds,[11] in which the odd electron is delocalized over the two molybdenum nuclei. The

(34) Zhuang, Q.; Fukuoka, A.; Fujimoto, T.; Tanaka, K.; Ichikawa, M. *J. Chem. Soc., Chem. Commun.* **1991**, 745.

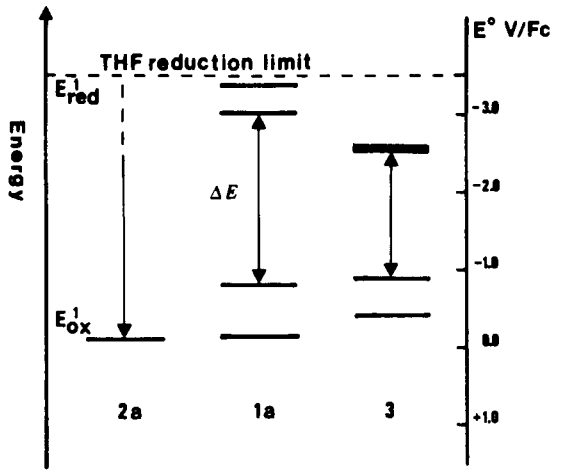

Figure 9. Potential-stick diagram showing the effect of the coordination mode on the value of the redox processes for the three complexes $[Mo_2(O_2CCH_3)_4]$ (**2a**), $[Mo_2(TMTAA)(O_2CCH_3)_2]$ (**1a**), and $[\{Mo(TMTAA)\}_2]$ (**3**). The difference between the first oxidation (E_{ox}^1) and first reduction (E_{red}^1) potentials, represented by ΔE, is an estimation of the HOMO–LUMO gap.

second oxidation step represents the transient formation of a $[Mo^{III}{}^{3}\!-\!Mo^{III}]^{2+}$ derivative, which decomposes very quickly, owing to the weakening of the bond order. Reduction steps are also evident at ca. −3.1 and −3.3 V for $[Mo_2(TMTAA)(O_2CR)_2]$ (**1**) and −2.5 V for $[\{Mo(TMTAA)\}_2]$ (**3**) and are ascribed to a two- or one-step reduction of $[Mo^{II}{}^{4}\!-\!Mo^{II}]$ into $[Mo^{I}{}^{3}\!-\!Mo^{I}]^{2-}$. In this case also, the decrease of the bond order is probably the origin of the instability of the reduced species. This precluded their characterization by any means and especially by ESR for the $[Mo^{II}{}^{3.5}\!-\!Mo^{I}]^{-}$ derivatives; this type of complex has been scarcely described and was difficult to characterize.[13b,c,d,35] The assignation of the site of the reduction, in the present case, is attested by the metallic character of the LUMO δ^* orbital involved, demonstrated in the theoretical analysis. Moreover, the differences between the oxidation and first reduction potentials calculated in the case of other Mo_2 complexes[13b,c,d] are in the same order of magnitude. In the previous work,[9] the misassignment of the first reduction process of $[\{Mo(TMTAA)\}_2]$ (**3**) to the reversible step located at ca. −0.82 V in THF was probably due to the presence of the oxidation product of this reaction by action of dioxygen. This was also observed here in some cases, but the effect of dioxygen on this family of compounds has not been scrutinized yet.

The present study shows that the occurrence and characteristics of these different redox steps are strictly under the control of the coordination mode of the $[Mo^{4}\!-\!Mo]$ moiety. These results are in keeping with those obtained for the previously described derivatives.[8,11-13] The strongest quadruple bond in $[Mo_2(O_2CR)_4]$, explained by the theoretical analysis, is illustrated by its redox behavior. This compound is the most difficult to oxidize to $[Mo^{II}{}^{3.5}\!-\!Mo^{III}]^{+}$, and this is the only redox process observed in the electrochemical window of common solvents. The electron-donating effect of the TMTAA ligand weakens the MoMo quadruple bond, and accordingly, the derivatives are easier to oxidize and to reduce; this effect is more pronounced when two TMTAA ligands are present (Table VII). However, it is difficult to make a comparison, because the coordination mode of the TMTAA ligand is different in the two complexes, **1** and **3**, as shown in Figure 2. The difference in the coordination mode of the TMTAA ligand is also illustrated by the ESR spectra. The low-temperature spectra reflect a same kind of symmetry, axial or isotropic, for the compounds $[Mo_2(O_2CR)_4]$ and $[\{Mo(TMTAA)\}_2]$, while the spectrum probably corresponds to orthorhombic character in $[Mo_2(TMTAA)(O_2CR)_2]$, probably owing to a lower symmetry. This is in good agreement with the schematical structures shown in Figure 2.

As far as the HOMO–LUMO gap is concerned, an observation similar to that obtained by the theoretical analysis can be made from the electrochemical measurements. The difference between the potential of the first oxidation process and the first reduction reaction is generally considered to provide an evaluation of the HOMO–LUMO gap, at least comparatively in a series. The values obtained in the present case, from Table VII, can be estimated as greater than 3.38 V in the case of $[Mo_2(O_2CR)_4]$ and equal to 2.30 and 1.67 V, respectively, for the derivatives $[Mo_2(TMTAA)(O_2CR)_2]$ and $[\{Mo(TMTAA)\}_2]$. This is illustrated by the diagram of Figure 9, which displays well the effect of the coordination mode on the electrochemical levels. Their ordering compares quite well with that obtained by the theoretical analysis and are in full agreement with the observed modulation of the $[Mo^{4}\!-\!Mo]$ bond strength by the type of coordination. The application of these observations to the reactivity of the $[Mo^{4}\!-\!Mo]$ unit toward small molecules, which recently found a renewal of interest,[34,36,37] is currently under investigation.

Acknowledgment. The CNRS (URA 322, URA 254, and URA 804) is acknowledged for support of this work. We thank Dr. A. Le Beuze for helpful comments and Pr. S. A. R. Knox for a careful reading of the manuscript.

Supplementary Material Available: For compound $[Mo_2(C_{22}H_{22}N_4)(O_2CCH_3)_2]$, tables giving crystal data and details of the structure determination, positional parameters, bond distances, bond angles, anisotropic thermal parameters for non-hydrogen atoms, equations of selected least-squares planes and interplanar angles, and torsional angles (11 pages). Ordering information is given on any current masthead page.

(35) Baxendale, J. H.; Garner, C. D.; Senior, R. G.; Sharpe, P. *J. Am. Chem. Soc.* **1976**, *98*, 637.

(36) Kerby, M. C.; Eichhorn, B. W.; Doviken, L.; Vollhardt, K. P. C. *Inorg. Chem.* **1991**, *30*, 156.

(37) Eichhorn, B. W.; Kerby, M. C.; Haushalter, R. C.; Vollhardt, K. P. C. *Inorg. Chem.* **1990**, *29*, 723.